

University of Groningen

Cellular homeostasis of Escherichia coli probed by super-resolution microscopy

van den Berg, Jonas

IMPORTANT NOTE: You are advised to consult the publisher's version (publisher's PDF) if you wish to cite from it. Please check the document version below.

Document Version

Publisher's PDF, also known as Version of record

Publication date:

2016

[Link to publication in University of Groningen/UMCG research database](#)

Citation for published version (APA):

van den Berg, J. (2016). *Cellular homeostasis of Escherichia coli probed by super-resolution microscopy*. [Thesis fully internal (DIV), University of Groningen]. Rijksuniversiteit Groningen.

Copyright

Other than for strictly personal use, it is not permitted to download or to forward/distribute the text or part of it without the consent of the author(s) and/or copyright holder(s), unless the work is under an open content license (like Creative Commons).

The publication may also be distributed here under the terms of Article 25fa of the Dutch Copyright Act, indicated by the "Taverne" license. More information can be found on the University of Groningen website: <https://www.rug.nl/library/open-access/self-archiving-pure/taverne-amendment>.

Take-down policy

If you believe that this document breaches copyright please contact us providing details, and we will remove access to the work immediately and investigate your claim.

Downloaded from the University of Groningen/UMCG research database (Pure): <http://www.rug.nl/research/portal>. For technical reasons the number of authors shown on this cover page is limited to 10 maximum.

Chapter 4

Cell volume and nutrient uptake of *Escherichia coli* at different growth rates

Jonas van den Berg, Ryan Henderson, Bert Poolman

Abstract

The size of enterobacteriaceae like *Escherichia coli* is directly affected by nutrient availability and follows the growth law, which implies that cell size is a function of growth rate. Volume homeostasis – and thus maintaining physicochemical parameters such as crowding, ionic strength and pH – is crucial for optimal functioning of the cell. We show that nutrient availability not only affects the volume of the whole cell, but also the distribution of volume over the cytoplasm and periplasm. We determined the volumes of the cytoplasm and the periplasm under different growth conditions, using photo-activated localization microscopy (PALM). In slow growing cells, the fraction of the cytoplasmic volume is decreased, and the periplasmic volume fraction is increased up to three times, along with an upregulation of periplasmic substrate-binding proteins (SBPs) of many ABC transporters. The concentration of the SBPs stays relatively constant when the volume changes are taken into account. We used FRAP to probe the lateral diffusion of a fluorescent protein in the periplasm and find that protein mobility is similar under all growth conditions and comparable to that of the cytoplasm. The diffusion measurements suggests that *E. coli* maintains the macromolecular crowding of the cytoplasm and periplasm at a constant level over a wide range of growth conditions, which impacts solute transport as shown for the uptake of maltose.

JvdB and BP designed the study, RH performed the uptake experiments, JvdB carried out the microbiology and microscopy, analyzed the data and wrote the manuscript.

Introduction

Bacterial cells have a defined shape that is dictated by the cell wall and the cytoskeleton [1, 2]. An *E. coli* cell has an average length of 1.6-3.1 μm [3], a width of 0.7-1 μm [3, 4] and the cell volume varies from 0.4 to 2 μm^3 [5]. Variations in cell dimensions exist for different *E. coli* genotypes, but the cell size is also known to be dependent on growth conditions. Cells growing in nutrient rich medium are longer and have a higher growth rate as compared to cells in minimal medium. In 1958, Schaechter postulated that cell size is a function of growth rate, independent of the medium used to achieve that growth rate [6]. This observation has become known as the growth law.

The size of Gram-negative bacteria is defined by the volume that is enclosed by the outer membrane (OM); the cytoplasmic volume is given by the boundary of the inner membrane (IM), and the difference between the two corresponds to the volume of the periplasm (see Figure 1A). Thus, the cell has to fulfill the task of dividing its total available space into two compartments, the cytoplasm and the periplasm. Estimates of the periplasmic volume in *E. coli* range from 10 to 40% of the total cell volume as determined by electron microscopy or fluorescent imaging [7-9]. Volume regulation in the cell is of crucial importance, since changes in volume directly affect parameters such as macromolecular crowding, ionic strength, pH, and membrane properties [10-13]. It is reasonable to assume that the cell maintains homeostasis for the cytoplasm as well as the periplasm.

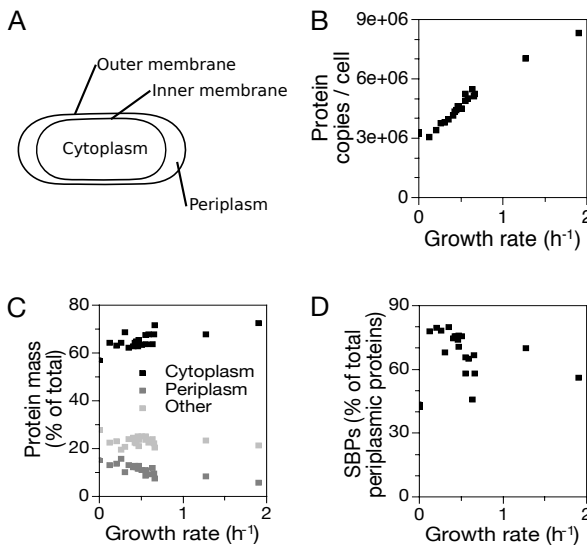


Figure 1: (A) Schematic representation of the *E. coli* cytoplasm and periplasm and the membranes separating both compartments. **(B)** Protein copy number per cell as a function of growth rate μ . **(C)** The amounts of cytoplasmic and periplasmic protein vary reciprocally with growth rate. **(D)** Substrate-binding proteins (SBPs) as fraction of the total amount of periplasmic proteins. Data for B, C and D are adapted from Schmidt et al. [17].

One important component of the periplasm is a layer of peptidoglycan (PG). The rigid PG network is tied to the outer membrane by Braun's lipoprotein, which anchors the PG layer to the inner leaflet of the OM, maintaining the structural strength of the *E. coli* cell to withstand a turgor pressure of approximately 3.5 atm [7, 14]. Furthermore, the periplasm contains high amounts of membrane-derived oligosaccharides (MDOs) [15], which are charged solutes too big to cross the outer membrane. They act as osmolytes and are the main contributors to keeping the periplasm isosmotic to the cytoplasm [7, 16]. Cells grown in low osmolarity medium require higher amounts of MDOs to match the higher turgor and to equilibrate the osmolarities of both compartments [16]. Large amounts of proteins are targeted to the periplasm to fulfill various functions, including substrate capture for transport, degradation of proteins, detoxification, and cell wall synthesis.

In a recent quantitative proteomic study, Schmidt and colleagues determined the abundance of more than 2,300 proteins under 22 growth conditions [17]. More than 95% of the total protein mass per cell was quantified. In Figure 1B we see that slow growing cells contain less protein overall. When proteins are classified based on their cellular localization, it is apparent that the protein biomass in the cytoplasm increases with growth rate μ relative to the periplasmic protein mass (Figure 1C).

Most of the proteins that are exported to the periplasm are substrate-binding proteins (SBPs) associated with ATP-binding cassette (ABC) transporters, and they make up 50 to 80% of the periplasmic protein mass (Figure 1D). Given the changes in protein mass of the cytoplasm and periplasm as a function of growth rate, we wondered if the volumes of these compartments would change accordingly and thus keep the actual protein concentrations constant. We also addressed the question as to whether a change in SBP concentration would affect the rate of solute uptake by the corresponding ABC transporter.

In this chapter, we quantify periplasmic and cytoplasmic volumes of *E. coli* under different growth conditions, using photo-activated localization microscopy (PALM). We find that the periplasmic volume fraction decreases and the cytoplasmic volume fraction increases with increasing growth rate. We performed fluorescence recovery after photobleaching (FRAP) to probe the mobility of a fluorescent protein targeted to the periplasm and used the lateral diffusion as an estimate of macromolecular crowding. We determined the rate of maltose uptake in *E. coli* as a function of the concentration of periplasmic maltose-binding protein (MBP). We find that at a given growth condition overexpression of MBP only moderately affects maltose uptake. However, cells

grown in minimal medium take up maltose significantly faster compared to fast growing cells, which indicates an overall increase in the expression of the components of the entire MalEFGK₂ transporter.

Material and Methods

Cloning

All plasmids and primers used in this study are listed in Table 1 and Table 2. The genes encoding periplasmic proteins (YPet or mEos3.2 with the signal sequence from TorA) were first inserted in a pBAD vector with the arabinose promoter and later subcloned in pACYC184, which carries the rhamnose promoter. The signal sequence *torA* was amplified with PCR (Phusion Polymerase), using genomic DNA of *E. coli* MG1655 as template, and *Nco*I and *Xma*I restriction sites were engineered 5' and 3', respectively. YPet and mEos3.2 (see Chapter 2) were amplified with 5' and 3' *Xma*I and *Xba*I site, respectively. The corresponding fragments were inserted into pBAD-LacY-eYFP, replacing the *lacY-eYFP* gene. To insert the fragments into pACYC184, the whole coding region of pBAD-TorA-YPet or pBAD-TorA-mEos3.2 were amplified and *Sal*I and *Bam*HI were introduced 5' and 3', respectively, and the corresponding fragments were inserted into pACYC-ThiT, replacing the original *thiT* gene.

Table 1: Plasmids used in this study.

Plasmid	<i>E. coli</i> expression strain	Antibiotic resistance ¹	Description
pACYC-TorA-YPet	MG1655	Cm	Periplasmic labeling
pACYC-TorA-mEos3.2	MG1655	Cm	Periplasmic labeling
pACYC-MalE	MG1655 $\Delta malQ$	Cm	Wild type MBP (MalE)
pBAD-mEos3.2	MG1655	Amp	Cytoplasmic labeling
pBAD-LacY-mEos2	MG1655	Amp	Inner membrane labeling
pCP20	MG1655	Amp, Cm	Flp recombinase
pEAW507	MG1655	Amp, Km	FRT-Km-FRT cassette,
pKD46	MG1655	Amp	Lambda red genes (<i>exo</i> , <i>bet</i> , <i>gam</i>), P _{araB} , <i>araC</i>
pRSET-mSA-YPet	BL21 (DE3)	Amp	Gift from S. Park
pRSET-mSA2-YPet	BL21 (DE3)	Amp	Purification for OM labeling

¹ Cm, chloramphenicol; Amp, ampicillin; Km, kanamycin

Table 2: Primers used in this study.

Number	Name	Sequence 5' to 3'
Colony PRC for <i>torA</i> and MPB		
4757	FP-NcoI-TorA	GCCATGCCATGGCCAATAACGATCTCTTTTCAGG
4758	TorA-XmaI-RP	ATATACCCGGGAGCCGCTTGCGCCGCAGTC
5984	SalI-MBP-FOR	CAGTCGGTTCGACCATGAAAATAAAAAACAGGTGCACGC
5985	MBP-BamHI-REV	GACTGTGGATCCTTACTTGGTGATACGAGTCTGC
Clone in pBAD-TorA-YPet and pBAD-TorA-mEos3.2		
4759	FP-TorA-YPet	CGATGCGTGCCCGGGTCTAAAGGTGAAGAATTATTC
4760	TorA-YPet-RP	CGCGGTCTAGACGGCTTAGAGCTCTTTGTACAATTC
4761	FP-TorA-mEos32	CATGTGCCCCGGGAGTGCGATTAAGCCAGACATGAAG
4762	TorA-mEos32_RP	GTCCTCTAGACGTTATCGTCTGGCATTGTCAGGCAATC
Recloning from pBAD in pACYC		
4982	pAC-TorA-YP-fw	GTGCGCGTCGACATGGCCAATAACGATCTCTTTTC
4983	pAC-TorA-YP-rev	CGGCGGATCCGTTAGAGCTCTTTGTACAATTC
4984	pAC-TorA-mE_rev	CAGTGGAATCCTTATCGTCTGGCATTGTGTCAG
Quikchange mSA-H-YPet (S25H)		
5283	PM-mSA-mSAH-for	CCGGCACGTGGTACAACCAGCATGGTTCTACCTTCACC
5284	PM-mSA-mSAH-rev	GCGGTAACGGTGAAGGTAGAACCATGCTGGTTGTACCACG
Construction of the <i>malQ</i> knockout		
6426	PAS-malQ-001-F	GATTATCAGGCTCGTATCTGGCAGGCAAAACGCTAAGGAA GTCGCGCCTTTTCGTCTTCAAGAATTC
6427	PAS-malQ-002-R	GATAAGACGCGTCAAGCATCGCATCCGGCATCAACCGCAC TGGCCACGATGCGTCCGGCGTA
6491	PAS-malQ-003-F	ATTTGCGAGCCTATGTAGAG
6492	PAS-malQ-004-R	TGGAAACCATTATCTCGGTGTG

To make the monomeric streptavidin fusion pRSET-mSA-H-YPet, we introduced the S25H mutation in the coding region of mSA (from S. Park [18]). Following the QuikChange protocol from Agilent, pRSET-mSA-YPet was used as a template with the primers 5283 and 5284 for PCR, using PfuTurbo polymerase. The plasmid was treated with *DpnI* before transformation into *E. coli* BL21 (DE3).

To obtain pACYC-MBP we amplified the *malE* gene from genomic DNA of *E. coli* MG1655, introducing *SalI* and *BamHI* restriction sites at the 5' and 3' ends, respectively. The PCR products were inserted into pACYC-ThiT, replacing the original *thiT* gene.

The *E. coli* MG1655 $\Delta malQ$ strain was constructed following the protocol of Datsenko and Wanner [19] with minor modifications. First, a linear DNA fragment, containing a kanamycin resistance gene, flanked by Flp recognition sites, was used to replace *malQ*. The plasmid pEAW507, carrying the FRT-KanR-wt FRT cassette, was used as a template for the PCR. The primers consisted of 41- and 45-bp sequences homologous to the flanking regions of *malQ* and 21-bp homologous to the FRT-kanR-wt FRT cassette. The recombining PCR product was digested with *DpnI* and electroporated in *E. coli*

MG1655, previously transformed with pKD46. Next, Kanamycin-resistant strains were screened for ampicillin sensitivity and transformed with pCP20 to remove the kanamycin cassette. All coding regions were confirmed by DNA sequencing.

Growth conditions for microscopy

Chemically competent cells of *E. coli* MG1655 were transformed with the plasmids listed in Table 1. Cells were cultured in EZ rich, defined medium (EZ-RDM from Teknova) or M9 minimal medium [17]. The media contained the carbon source indicated in Table 3 and were supplemented with 100 $\mu\text{g/mL}$ ampicillin (Sigma Aldrich) or 32 $\mu\text{g/mL}$ chloramphenicol (Sigma Aldrich). All media were adjusted to 0.3 ± 0.02 Osm with NaCl. The cells were grown at 37 °C and 200 rpm shaking. The growth rates shown in Table 3 were determined by fitting OD₆₀₀ data as a function of time with a single exponential. At a final OD₆₀₀ of 0.25 – 0.5 cells were prepared for microscopy.

Table 3: Growth medium with corresponding *E. coli* doubling times at 37 °C.

Growth medium	Concentration of carbon source (mg/mL)	Doubling time (min)	Growth rate (h ⁻¹)
EZ-glycerol	2.0	32	1.31
M9-glycerol	2.2	100	0.42
M9-galactose	2.3	120	0.35
M9-acetate	3.5	200	0.21

Sample preparation for microscopy

Cover slides (Carl Roth, LH26.1) were cleaned in 5 M KOH for 40 min in a sonication bath, followed by extensive washing with MQ. Next, the coverlids were rinsed in acetone and allowed to dry completely, before they were cleaned in a Plasma Cleaner for 10 min. Cleaned cover slides were coated with a 2% (v/v) solution of (3-Aminopropyl)triethoxysilane (Sigma Aldrich) in acetone for 20 minutes. Then, they were washed in MQ, rinsed in acetone and allowed to dry again. Cells in the exponential phase of growth were concentrated to OD₆₀₀~1 and 25 μL were dispersed on a coated cover slide with a second cleaned cover slide on top. All PALM measurements were carried out at room temperature. For the FRAP measurement, the Plasma Cleaner was not used and cells were not concentrated before imaging.

PALM setup

For single molecule imaging a home-built inverted microscope based on an Olympus IX-81 with a high numerical aperture objective (100 X, NA = 1.49, oil

immersion, Olympus, UAp0) was used. Imaging was performed in semi-TIRF mode and fluorescence was recorded using an electron multiplying charge coupled device (EM-CCD camera) from Hamamatsu, Japan, model C9100-13. Solid-state lasers were from Coherent (Santa Clara, USA): 514 nm (Sapphire 514-100CW), 405 nm (Cube, 100 mW) and 561 nm (Sapphire 561, 100 mW). The laser power for activation (405 nm) was set to ~ 10 mW/cm², and for readout out (561 nm) to ~ 1 kW/cm². Laser power for YPet (514 nm) was set to ~ 2 kW/cm². Laser beams were collimated with lenses and combined using dichroic mirrors. To activate mEos3.2 and mEos2 molecules, a pulsed laser was used for illumination. To detect single molecules, typically 150-250 cycles of photoactivation were repeated with each cycle consisting of 1 frame for mEos3.2 activation and subsequent 19 frames for read-out. The exposure time of each frame was 31 ms.

PALM data analysis

The acquired movies were analyzed with a home-written ImageJ plugin. In the reconstructed images each fluorescent molecule was represented as a single spot at its determined coordinates with a brightness that corresponds to the localization accuracy.

Periplasmic labeling

For super-resolution microscopy and FRAP experiments, periplasmic labeling was achieved by expressing the fluorescent proteins YPet and mEos3.2 attached to the TorA signal sequence, using the pACYC vector with the *rha* promoter. Induction was done for 1 h with 0.01% (w/v) *L*-rhamnose. Fast growing cells in EZ-glycerol were induced for 1.5 h. A post-induction time was introduced to ensure complete export of the fluorescent protein to the periplasm. After the induction period, cells were washed twice with fresh medium and resuspended in the same medium without inducer and allowed to continue growing, before they were prepared for microscopy. The post-induction time was 1 h, if not stated otherwise.

Dual-color labeling of cells

To label the periplasm and cytoplasm simultaneously, competent cells of *E. coli* MG1655 were transformed with two compatible plasmids, pACYC for expression of periplasmic TorA-YPet and pBAD for expression of cytoplasmic mEos3.2. For PALM, cells were grown in EZ-glycerol in the presence of ampicillin plus chloramphenicol. First, TorA-YPet was induced for 1.5 h with 0.01% (w/v) *L*-rhamnose. Then, the *L*-rhamnose was removed and 0.01% (w/v) *L*-arabinose was added for 1 h, combining post-induction time for periplasmic labeling (TorA-YPet) with expression of cytoplasmic mEos3.2.

Expression and purification of monomeric streptavidin fusion

First mSA-H-YPet – a monomeric variant of streptavidin (mSA-H) fused to the fluorescent protein YPet [20] – was purified using a protocol for proteins in inclusion bodies, adapted from Lim et al. [18]. *E. coli* BL21(DE3) harboring pRSET-mSA-H-YPet was grown in 0.5 L LB medium containing 100 µg/mL ampicillin at 37 °C. At OD₆₀₀ ~ 0.8 cells were induced with 0.1 mM IPTG for 4 h until the OD₆₀₀ reached ~4. Cells were centrifuged (20 min, 4 °C, 27,000xg) and the pellet was frozen in liquid nitrogen. The next day, the pellet was resuspended in 10 mL Bacterial Protein Extraction Reagent (B-PER™ from ThermoFisher Scientific) and centrifuged again (20 min, 4 °C, 27,000xg). Now, the pellet was resuspended in 20 mL B-PER plus 0.2 mg/mL lysozyme and 0.1 mg/mL DNase and incubated for 30 min at room temperature. 40 mL wash buffer WB1 (50 mM Tris-HCl, pH 8.0, 100 mM NaCl plus 0.5% Triton X-100) was added and the suspension were mixed until the solution became clear (~20 min). The inclusion bodies were sedimented (20 min, 4 °C, 27,000xg) and the pellet was washed twice with 30 mL WB1. Next, the pellet was resuspended in 3 mL solubilization buffer SB (6 M guanidine hydrochloride, 50 mM Tris-HCl, pH 8.0 plus 100 mM NaCl). The insoluble fraction was removed by centrifugation (20 min, 4 °C, 5,000xg) and the supernatant was added to 0.5 mL prewashed Ni-Sepharose beads and incubated for 1 h at 4 °C with mild shaking. Then, the resin was washed with wash buffer WB2 (6 M guanidine hydrochloride, 50 mM Tris-HCl, pH 8.0, 150 mM NaCl plus 25 mM imidazole) and eluted with elution buffer EB (same as WB2 but with 300 mM instead of 25 mM imidazole). The yellow elution fractions were added very slowly to 40 mL ice-cold refolding buffer RB (50 mM Tris-HCl, pH 8.0, 150 mM NaCl, 0.3 mg/mL *D*-biotin 0.2 mg/mL oxidized glutathione plus 1 mg/mL reduced glutathione) under vigorous stirring with a magnetic mixer. Precipitates were removed by centrifugation (20 min, 4 °C, 5000xg) and the supernatant was added to a Sartorius centrifugal filter with a 10 kDa cutoff (Vivaspin 20, VS2002, 10.000MWCO PES) to concentrate the refolded protein to a final volume of ~1.5 mL). The concentrated protein was then dialyzed 3 times with a Servapor dialysis tube (Serva, MWCO 12,000-14,000) against 3x1 L dialysis buffer DB (50 mM Tris-HCl, pH 8.0, plus 150 mM NaCl) at 4 °C over a period of 3 days. Finally, the buffer was exchanged to PBS with an Illustra™ NAP10 column (GE Healthcare). The final concentration was 0.69 mg/mL mSA-H-YPet in PBS.

Determination of periplasmic volume

To determine the periplasmic volume V_{PP} we measured the cytoplasmic volume V_{CP} by labeling the inner membrane with LacY-mEos2 and the total cell

volume V_{cell} by labeling the outer membrane with mSA-H-YPet. The periplasmic volume was calculated from the difference: $V_{PP} = V_{cell} - V_{CP}$. *E. coli* MG1655 harboring pBAD-LacY-mEos2 were grown in the various media listed in Table 3 and induced with 0.01% *L*-arabinose. After 1 h of expression, 0.5 mL of the culture was centrifuged (11.000xg for 1 min) and washed twice with isoosmotic PBS. The cell surface was biotinylated by resuspending the pellet in 1 mg/mL EZ-Link Sulfo-NHS-LC-Biotin (Thermo Scientific) dissolved in PBS (pH = 7.6) and incubating at RT for 30 min with mild shaking. Cells were washed twice in PBS supplemented with 100 mM glycine to quench the remaining NHS-LC-biotin. Finally, the cells were resuspended in 100 μ L purified mSA-H-YPet ($c = 0.14$ mg/mL) and incubated for 5 min. The cells were washed twice in PBS and prepared for PALM. It is important to note that all washing and reaction buffers for labeling the outer membrane were isoosmotic to the growth media (0.3 ± 0.02 Osm).

To calculate the volume, we first tracked the membranes in the PALM reconstruction with a segmented line in ImageJ to obtain the XY coordinates of the cell membrane. The cell was then divided into two halves with the long axis spanning from one pole to the other. The XY coordinates from one half of the cell were transformed in R (RStudio, Inc., Boston, MA), such that the long cell axis was superimposed on the X-axis of the coordinate system. The cell volume was calculated from the solid of revolution (i.e. a solid created by rotating the transformed XY coordinates around the X axis), using the Simpspon's rule (see Figure 5B for graphical explanation).

FRAP

To determine the lateral diffusion of YPet in the periplasm, we grew *E. coli* MG1655 bearing the plasmid pACYC-TorA-YPet and induced for 1 h (or 1.5 h for cells growing in EZ-glycerol) with 0.01% (v/v) *L*-rhamnose. After 1h post-induction the cells were prepared for microscopy. FRAP was recorded on a laser-scanning confocal microscope (Zeiss LSM 710, Carl Zeiss, Jena, Germany C-apochromat 40 \times /1.20 w Korr M27 water immersion objective with NA of 1.2). The temperature was set to 37 $^{\circ}$ C. Selected cells were magnified 35 times and a squared region of around 0.5 μ m² on one pole of the cell was bleached with a high intensity 488 nm laser for 3 frames and consequently imaged with lower laser power for 197 frames with exposure time of 9.45 ms. Fluorescence emission was collected from 493 to 797 nm. Diffusion coefficients were calculated as described in [21]. In brief, a line was drawn from one cell pole to the other. The fluorescence intensity along that line was plotted for each frame during fluorescence recovery. An example of the resulting heat map is shown in

Figure 6B. The data was analyzed with home-written software and the analysis is based on the 1-dimensional diffusion equation:

$$\frac{\partial c(x, t)}{\partial t} = D \frac{\partial^2 c(x, t)}{\partial x^2}$$

with boundary conditions:

$$\frac{\partial c(x, t)}{\partial t} = 0$$

where c is fluorescence intensity at position x and time t , and D is the lateral diffusion coefficient.

¹⁴C-Maltose uptake experiments

For the uptake experiments, we used *E. coli* MG1655 $\Delta malQ$; a strain that cannot metabolize maltose because the gene encoding maltase was deleted. We grew *E. coli* MG1655 $\Delta malQ$ with pACYC-MalE in EZ-glycerol or M9-acetate (i) in the absence of inducer and (ii) by adding 0.01% (w/v) *L*-rhamnose to overexpress the *malE*, resulting in four different cultures for the uptake experiment.

In the exponential phase of growth (OD₆₀₀ of 0.4), cells were harvested by centrifugation, washed twice with PBS plus 0.2% (w/v) glycerol and concentrated to an OD₆₀₀ of 10 in the same buffer. For the uptake experiment, cells were diluted 1:10 in PBS plus 0.2% (w/v) glycerol and were incubated for 1 minute at 37 °C. The uptake reaction was started by adding ¹⁴C-maltose to a final concentration of 10 μM, 50 μM or 250 μM. At given time intervals, 50 μL samples quenched in ice-cold PBS and rapidly filtered over a 0.45 μm pore size nitrocellulose filter (GE Healthcare, Little Chalfont, UK). Filters were washed once with 2mL ice-cold PBS. Filters were then dissolved in 2mL liquid scintillation solution (Emulsifier^{plus}, PerkinElmer, Waltham, MA, USA) and the radioactivity on the filters was determined by liquid scintillation counting (Tri-Carb 2800TR liquid scintillation analyzer, PerkinElmer). The precise cell numbers were obtained by counting cells in a flow cytometer (BD AccuriTM C6). Expression levels of maltose-binding protein were determined by Western blotting. For this, 130 μL of the concentrated cell suspension were pelleted and lysed in B-PER (ThermoFisher Scientific) with 0.1 mg/mL DNase, 1mM MgSO₄ and protease inhibitor oComplete (Roche) for 15 min. The lysate was centrifuged at 4 °C for 15 min at 20,000xg and the supernatant was loaded on a 12.5% SDS-PAGE gel. Proteins were transferred to a PVDF membrane and the Western Blot was developed with an α-MBP antibody (NEB), using a titer of 1:10,000.

Results

To determine the volume of the *E. coli* cytoplasm and periplasm, one requires high-resolution imaging with a resolution well below the diffraction limit of light. We used two strategies based on photo-activated light microscopy (PALM): (i) by differential labeling of the cytoplasm and periplasm; and (ii) by differential labeling of the inner and the outer membrane.

Labeling of periplasm and cytoplasm

To label the periplasm the highlighter fluorescent proteins YPet or mEos3.2 (FP) were fused to an N-terminal signal sequence, TorA, which was derived from the *E. coli* periplasmic trimethylamine N-oxide reductase [22]. The TorA signal sequence is recognized by the twin-arginine translocation (TAT) pathway, which can export fully folded proteins to the periplasm [23]. As previously reported [24, 25], the export of a fluorescent protein to the periplasm is rather slow. The *L*-rhamnose inducible *rha* promoter of pACYC is relatively weak, which reduces the risk of overburden the TAT pathway.

We first optimized the expression conditions for labeling of the periplasm, using pACYC-TorA-YPet. In order to export all fluorescent proteins to the periplasm, we introduced a post-induction time in which the cells were able to continue growing in the absence of inducer. At different post-induction times we imaged the cells to determine the completion of the translocation of matured protein from the cytoplasm to the periplasm. Cross sections were drawn along the indicated lines for ~10 cells with equal length (see Figure 2A), and an averaged intensity profile was plotted along the long and the short axis of the cell (Figure 2B). Immediately, after induction a clear periplasmic signal was visible at the poles of the cell. After 30 minutes the periplasm was also clearly visible at the cylindrical part of the cell, indicating an increasing amount of exported YPet.

After 60 minutes of post-induction time the profile did not change significantly anymore and longer post-induction times lead to a loss of fluorescent signal due to the distribution of YPet over new generations of cells. Figure 2C and D show representative images of cells after 0 and 60 minutes, respectively. We found an *L*-rhamnose concentration of 0.01% and a post-induction time of 1h yields optimal labeling. Figure 3A shows a PALM reconstruction of TorA-YPet after post-induction time optimization. YPet showed increased localizations at the cell poles, which means that the distance between the inner and outer membrane is bigger at the end caps. TorA-mEos3.2 was not exported well to the periplasm (Figure 3B); hence we used TorA-YPet for our further studies.

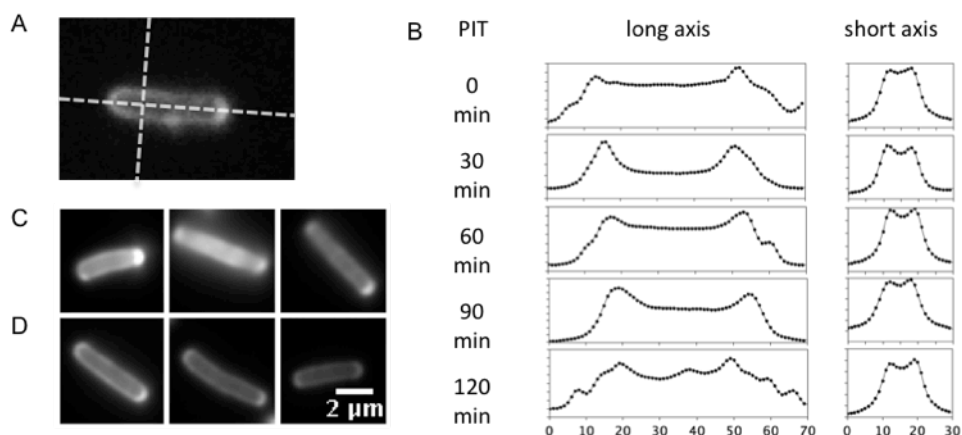


Figure 2: Export of TorA-YPet after different post-induction times. **(A)** Cross sections of resolution-limited cell images were made by plotting the intensity along the drawn lines. **(B)** Fluorescence intensity profile along the long and the short axis of the cell. **(C)** Export of YPet after 0 and **(D)** 60 min of post-induction time. We used an *L*-rhamnose concentration of 0.01% to induce for 1h and a post-induction time of 1h.

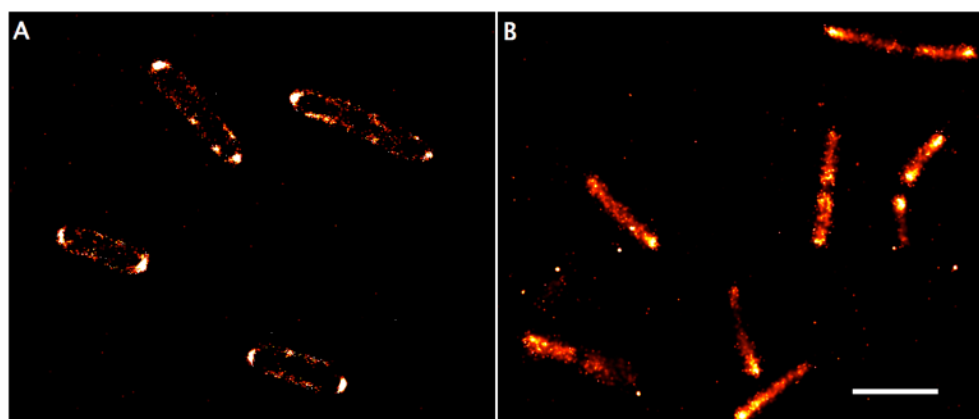


Figure 3: PALM reconstructions of **(A)** TorA-YPet and **(B)** TorA-mEos3.2 after 1h of post-induction time. YPet can be found in the periplasm, whereas the signal from mEos3.2 is clearly derived from the cytoplasm, showing no export to the periplasm. Scale bar: 2 µm.

Having optimized the conditions for periplasmic labeling, we transformed pACYC-TorA-YPet and pBAD-mEos3.2 in *E. coli* MG1655 to label both compartments. Early exponential phase cells grown in EZ-glycerol ($OD_{600} \sim 0.05$) were first induced with 0.01% (w/v) *L*-rhamnose for 1.5 h. Next, the cells were washed to remove *L*-rhamnose and resuspended in fresh medium with *L*-arabinose, combining post-induction time for periplasmic labeling with

expression of cytoplasmic mEos3.2. In Figure 4 we see dual color PALM images of both *E. coli* compartments. The heterogeneous expression of fluorescent proteins from pBAD and pACYC plasmids resulted in many cells having either only cytoplasmic or only periplasmic labeling. The separation between the

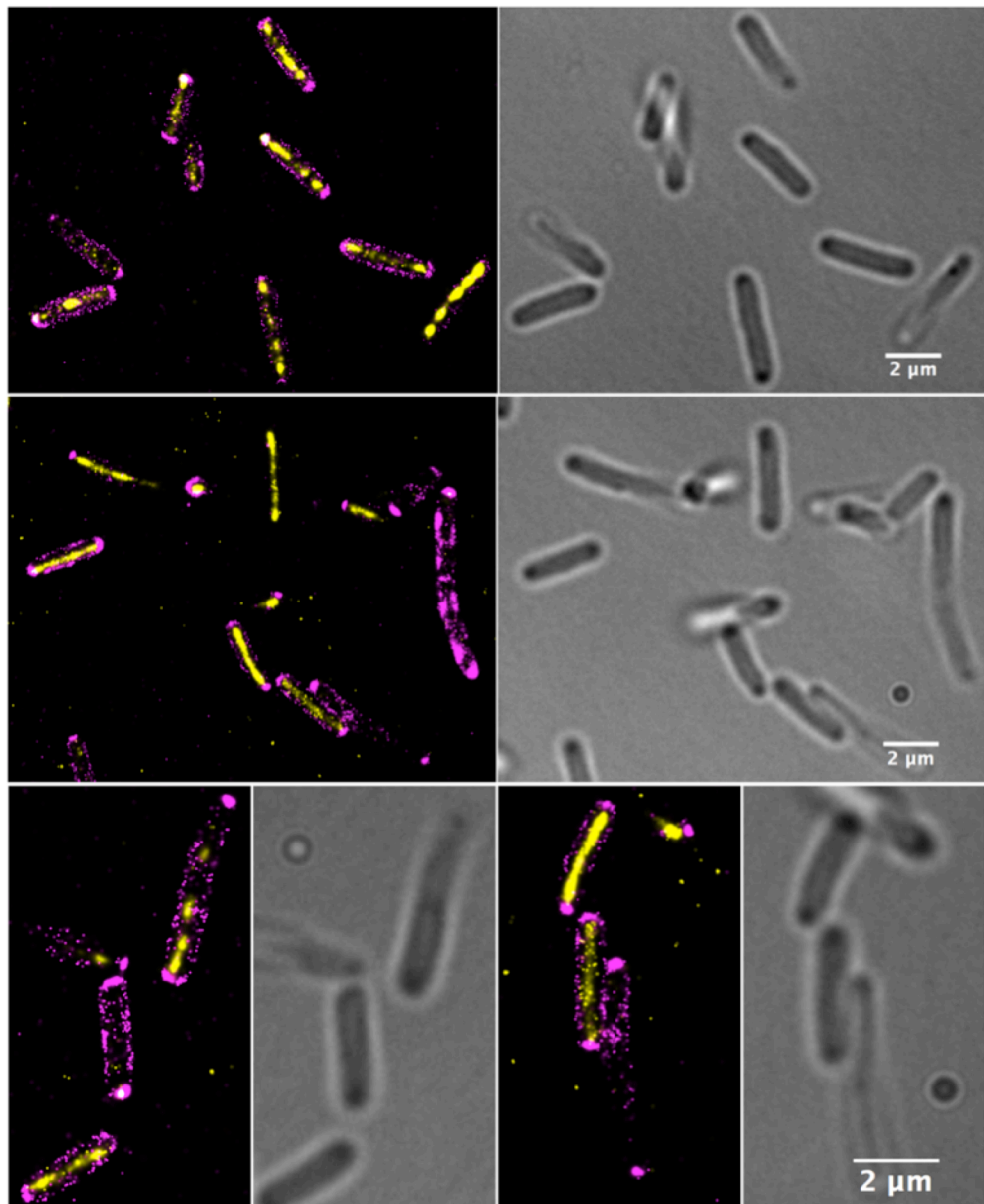


Figure 4: Dual-color PALM to visualize the periplasm and cytoplasm of *E. coli* MG1655. TorA-YPet was expressed from the *rha* promoter in pACYC and exported to the periplasm using the TAT pathway (magenta). mEos3.2 was expressed from the *ara* promoter in pBAD and is localized in the cytoplasm (yellow).

cytoplasm and the periplasm was not clearly visible, which precluded accurate determination of the volumes of both compartments. We therefore devised a different strategy based on differential membrane labeling to determine the volume of the cytoplasm and periplasm.

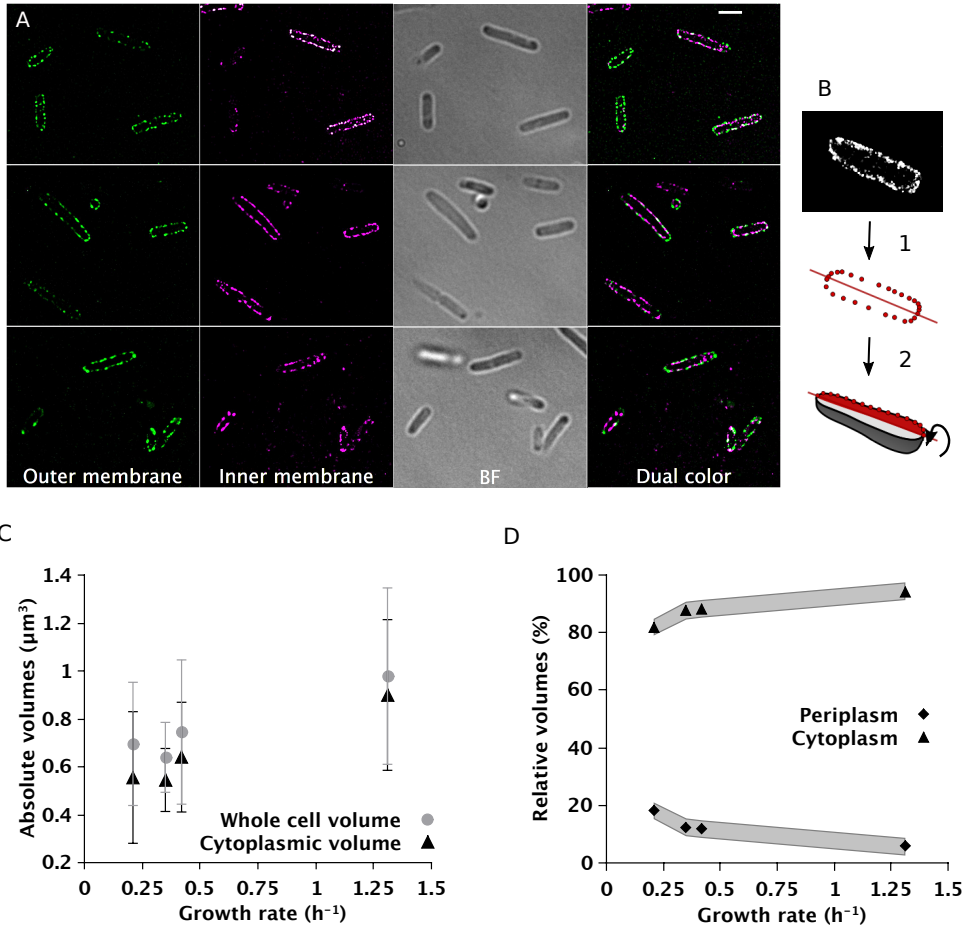


Figure 5: Inner and outer membrane labeling with photoactivatable fluorophores reveals the dimensions of the cytoplasm and periplasm under different growth conditions. **(A)** PALM reconstruction of outer and inner membrane of *E. coli* MG1655 grown in EZ-glycerol with corresponding bright field image and an overlay of both membranes. Scale bar = 2 μm . **(B)** To estimate the volume from PALM images, first the outlines of the membrane were tracked in ImageJ and the cell was divided into two halves (1). Then, the cell volume was calculated as the volume of the solid of revolution (i.e. a solid created by rotating the transformed XY coordinates around the X axis), using the Simpson's rule (2). **(C)** Absolute and **(D)** relative volumes of both compartments as a function of growth rate; see Table 3 for the growth conditions. Grey areas in **(D)** represent the range of relative volumes assuming an overestimation of the periplasmic width of 10 nm \pm 5 nm. Error bars represent the standard deviation between individual cytoplasmic or whole cell volume determinations.

Volume determination via differential membrane labeling

Next, we labeled the inner membrane by expressing LacY-mEos2, which provided an estimate of the cytoplasmic volume. The outer membrane was labeled by biotinylating the cell surface and adding purified mSA-H-YPet; a monomeric variant of streptavidin [20] (see Methods section) fused to a fluorescent protein. We chose four growth conditions with *E. coli* doubling times ranging from 32 to 200 min and performed dual-color PALM. Representative PALM images for fast growing cells are shown in Figure 5A. Since LacY-mEos2 has the fluorophore on the cytoplasmic face of the IM and mSA-H-YPet has the fluorophore on the outer surface of the OM (and each at a distance of a few nm from the membrane), the distance between IM and OM will be overestimated by approximately 10 nm, which leads to an underestimation of the cytoplasmic volume and an overestimation of the whole cell volume (see Discussion). The graphs in Figure 5C and D are corrected for these anomalies and show absolute and relative volumes of both compartments, respectively. The size of the periplasm is dependent on the growth condition. With decreasing growth rate μ the fraction of the periplasmic volume increased approximately three times when comparing to the condition of fastest growth. The width of the cell was consistently $0.7 \mu\text{m} \pm 0.07 \mu\text{m}$ and the averaged distance between inner and outer membrane is 16 ± 14 nm along the cylindrical part of the cell over all growth conditions.

Periplasmic YPet diffusion as a measure of crowding

To measure the crowding conditions in the periplasm we have attempted to target the previously developed FRET-based crowding sensor [26] to the *E. coli* periplasm, using the TorA signal sequence and controlled expression. However, the multidomain sensor proved too complex for efficient export by the TAT pathway (see Chapter 5). We therefore estimated the apparent crowding of the periplasm from the lateral diffusion of YPet, using fluorescence recovery after photobleaching (FRAP). Figure 6A shows a representative *E. coli* cell that was bleached on one side. Images were acquired at relatively low spatial resolution to allow shorter exposure times. Recovery of fluorescence can be seen in the subsequent images at given times after the photobleaching. Figure 6B shows the distribution of fluorescence at different time points during the FRAP experiment. The data show that fluorescence fully recovers, indicating that YPet does not form aggregates in the periplasm.

The distributions of the lateral diffusion coefficients of TorA-YPet in the periplasm of *E. coli* are presented in Figure 7. The average diffusion coefficients are given in Table 4. We find that the mobility of periplasmic YPet

in cells grown in rich media is somewhat faster than that of slow growing cells. Given that the differences in diffusion coefficients are relatively small, we infer that macromolecular crowding of the periplasm is relatively constant.

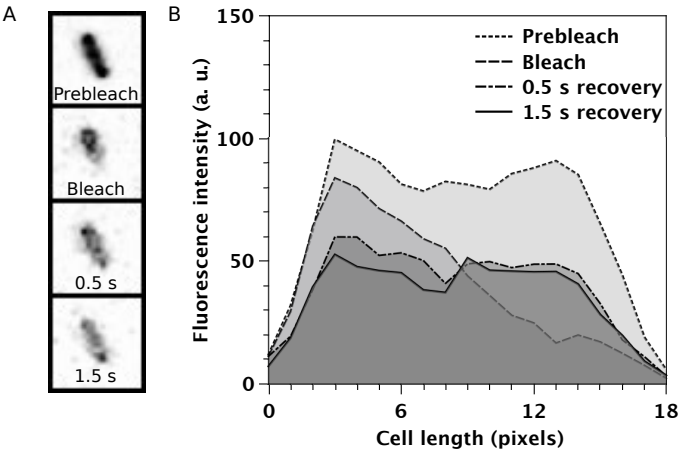


Figure 6: Fluorescence recovery after photobleaching in *E. coli* cells expressing TorA-YPet. Cells were grown in EZ-Glycerol and induced with 0.01% *L*-rhamnose for 1h, followed by a post-induction time of 1h prior to FRAP measurements. **(A)** Fluorescence of a cell before and at different time steps after bleaching. **(B)** Intensity profiles along the long axis of the cell before photobleaching and at different time points during recovery.

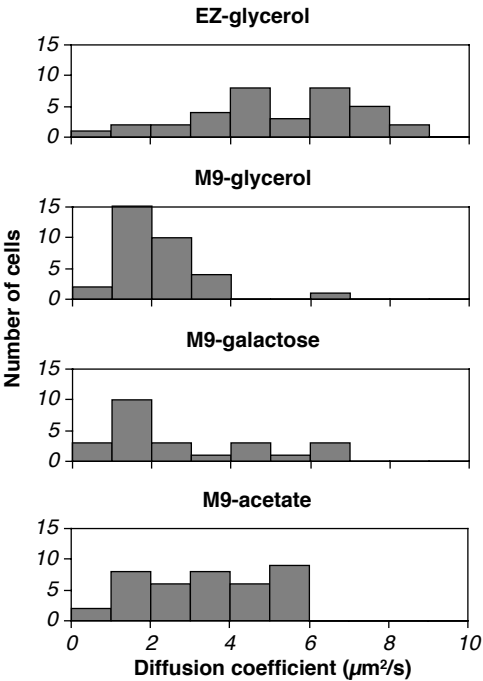


Figure 7: Distribution of periplasmic diffusion coefficients of TorA-YPet in *E. coli* MG1655 cells grown in different media. YPet was allowed to mature and be exported to the periplasm, and diffusion measurements were done by FRAP. Histograms were obtained by analyzing cells measured on different days.

Table 4: Average lateral diffusion coefficients D_{AV} with standard deviation SD of TorA-YPet in the periplasm of *E. coli*.

Growth medium	Growth rate (h ⁻¹)	D_{AV} (μm ² /s)	SD (μm ² /s)	Number of cells
EZ-glycerol	1.31	5.1	2.0	36
M9-glycerol	0.42	2.2	1.0	33
M9-galactose	0.35	2.7	2.1	24
M9-acetate	0.21	3.5	1.6	25

Maltose uptake in different growth conditions

The increase in periplasmic volume in slow growing cells correlates with upregulation of SBPs [17]. In fact, the overall concentration of periplasmic proteins, of which 50-80% correspond to SBPs, is relatively constant as a function of growth rate (see Discussion). We thus wondered what the impact of a change in SBP concentration would be for the transport via a given ABC transporter. We tested the effect of varying SBP concentration on maltose transport for cells grown in rich and in minimal media. To determine genuine maltose transport activity we deleted the gene coding for amyloamylase (*malQ*) and induced the maltose operon of *E. coli* MG1655 $\Delta malQ$ by addition of 10 μM maltose to the growth medium. We varied the level of maltose-binding protein (MBP, MalE) by coexpressing *malE* from a plasmid using the *rha* promoter.

The dissociation constant, K_D , of MBP for maltose is 1 μM and the affinity constant of maltose transport, K_m , is similar [27]. On the other hand, the K_D of membrane-embedded MalFG for liganded MBP is 25-50 μM [28], which is in the range of the periplasmic concentrations of MBP in non-induced cells. Transport of maltose is expected to be sensitive to the actual concentration of MBP. At low maltose concentration the uptake could potentially be limited by diffusion of maltose through maltoporin (LamB) in the outer membrane of *E. coli*. We thus determined the rate of uptake at 10, 50 and 250 μM ¹⁴C-maltose and found no differences, indicating that we are probing the activity of the maltose ABC transporter (MalEFGK₂) rather diffusion through maltoporin.

Figure 8A shows that for cells grown in EZ-glycerol, a 1.5-fold increase in MBP (see Figure 8B and C) only marginally increased maltose transport. For cells grown in M9-acetate we were able to increase the amount of MBP by a factor of ~2.5, which enhanced the rate of maltose uptake by about 25%, based on the slope in Figure 8A. These data indicate that in minimal medium the rate of maltose uptake is limited by the concentration of MBP in the periplasm. The absolute rate of maltose transport in EZ-glycerol grown cells is lower than in M9-acetate grown cells. Slight overexpression of MBP in fast growing cells

adjusts the levels of MBP to the same level as in minimal media, without increasing the uptake, which likely reflects a lower expression of the transporter as a whole.

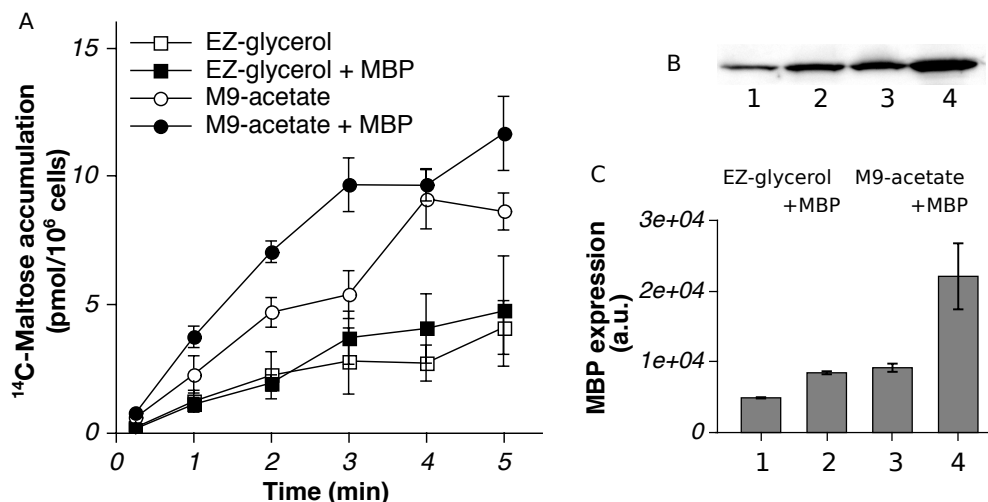


Figure 8: (A) ^{14}C -maltose uptake in cells grown in rich (EZ-glycerol) and minimal (M9-acetate) media. The level of maltose-binding protein (MBP) was varied by expressing *malE* under the control of the *rha* promoter of pACYC. Error bars represent the standard deviation of three replicates. (B) MBP was detected on a Western Blot with anti-MBP for cells grown in (1) EZ-glycerol, (2) EZ-glycerol + MBP (3) M9-acetate and (4) M9-acetate + MBP. Samples were corrected for OD_{600} . (C) Quantification of the MBP expression levels from Western blots; legends are the same as in (B) and error represent the standard deviation of two replicates.

Discussion

Whereas most biochemical reactions take place in the cytoplasm, the periplasm serves as a protecting shell where the first stage of nutrient uptake (solute binding) takes place. In a recent quantitative proteomics study, Schmidt et al. observed that the amount of cytoplasmic proteins increases and the amount of periplasmic proteins decreases as a function of growth rate [17]. We now determined the accompanying changes in the volumes of the cytoplasmic and periplasmic compartments and find that they vary oppositely with growth. In fact, if we correlate the protein abundance from the proteomics data to the volume measurements, we find that the overall protein concentration of cytoplasm and periplasm stays relatively constant (see Figure 9).

Volume determination of bacterial cells is challenging due to their small size. Electron microscopy has been used before to observe changes in the volume of

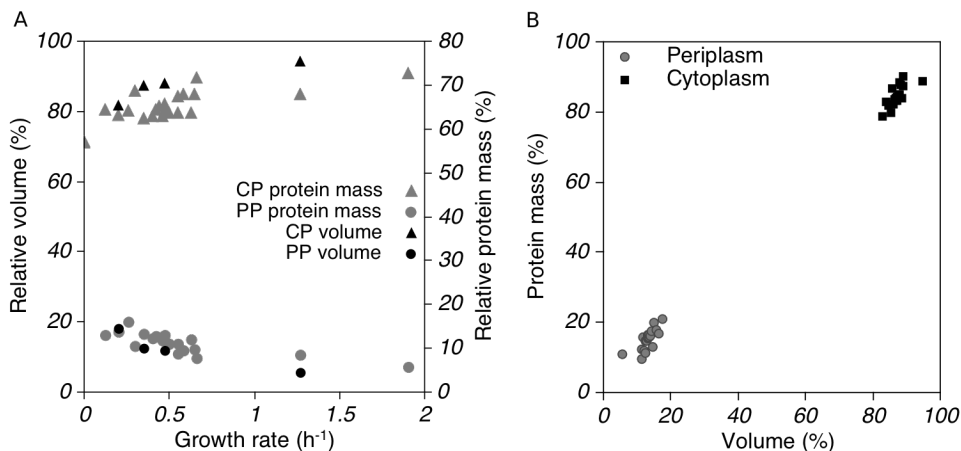


Figure 9: (A) *E. coli* protein mass in different cellular compartments (relative to all *E. coli* proteins, including membrane proteins) and relative volumes of cytoplasm and periplasm obtained by dual-color PALM (this study). (B) Protein mass of cytoplasm and periplasm as function of the corresponding volumes. The compartmental volumes in (A) were fitted with a linear equation to calculate the volumes for the other growth rates; the proteomic data were taken from [17].

the cytoplasm and periplasm [7, 8], but does not permit imaging of live cells and freezing or staining of cells can lead to artifacts. We show that PALM is a suitable method to determine the volumes of the cytoplasm and periplasm. We find that the best strategy for determination of the volumes is based on differential labeling of the outer and inner membrane. We used monomeric streptavidin mSA-H fused to YPet to label the outer membrane of biotinylated cells, and LacY-mEos2 to label the inner membrane. Because Sulfo-NHS-LC biotin has a 2 nm flexible spacer arm, mSA-H has a diameter of ~1 nm (~15 kDa) and YPet is connected to mSA-H via a flexible linker, the fluorophore will be a few nm distal of the OM. Similarly, mEos3.2 is a 1-2 nm distal of the IM but now on the inside. Another factor that contributes to the overestimation of the volume of the periplasm is the thickness of the membranes, which is ~4 nm for the IM and OM. We thus conclude that our data obtained from dual color PALM overestimates the width of the periplasmic space by about 10 nm.

When we correct our PALM localizations for this overestimate, we find that the width of the periplasm at the long axis of the cell is ~16 nm. The width of the periplasm has been reported in the range of 11-21 nm [29, 30], which is in good agreement to our data, however larger values (~45 nm) have been reported by Pilizota et al. [9] and T. Kubori et al. (for *Salmonella typhimurium*) [31]. On the basis of the dimensions of the tripartite RND-type ‘transenvelope’

transporter systems that span the inner membrane, periplasm and outer membrane, the width of the periplasm should (at least locally) be 14 nm [32, 33].

The combined quantitative proteomics-volume measurements data in Figure 9A indicate that changes in protein mass and volume coincide. The protein concentrations of the cytoplasm and periplasm stay relatively constant as a function of growth rate, indicating that macromolecular crowding is kept relatively constant (see Figure 9B). However, other macromolecules contribute to crowding, like nucleic acids, which are absent in the periplasm. Moreover, the molecular mass of periplasmic proteins is in the range of 25-80 kDa, whereas cytoplasmic biomacromolecules vary from <10 kDa to >2000 kDa [17] and different sized proteins will contribute differently to macromolecular crowding. We have tried to compare the crowding of cytoplasm and periplasm using a recently developed FRET-based sensor [26]. Unfortunately, we did not succeed in targeting sufficient amounts of the crowding sensor to the periplasm (see Chapter 5).

We thus evaluated macromolecular crowding of the periplasm on the basis of lateral diffusion measurements, using FRAP of TorA-YPet. Most fluorescent proteins do not fold in the periplasm. For that reason, we used the TAT pathway to export fully folded and matured TorA-YPet. To ensure complete export, we introduced a post-induction time. The signal emanating from cytoplasmic TorA-YPet is negligible after 1 h of post-induction time. The group of Weisshaar [25] used a similar approach, and from simulations they conclude that 95% of all FPs are found in the periplasm under their experimental conditions.

The lateral diffusion coefficients are in the range of 2-5 $\mu\text{m}^2/\text{s}$, which is in good agreement with Sochacki et al. [25]. The mobility of periplasmic YPet is comparable to that of fluorescent proteins in the cytoplasm, for which diffusion coefficients of 3-6 $\mu\text{m}^2/\text{s}$ have been determined [10, 34, 35]. We find that for cells growing in minimal media the periplasmic diffusion is roughly 2-fold slower compared to fast growing cells. The lateral diffusion of fluorescent proteins is an indirect way of measuring macromolecular crowding [36], additionally is not clear how the presence of the peptidoglycan affects protein mobility or if the diffusion is confined due to the narrow width of the periplasm along the long axis of the cell. Therefore we cannot directly compare the diffusion measurements between both compartments.

When nutrient availability is limited, cells possibly may invest more energy in nutrient uptake at the expense of growth promoting processes. The

upregulation of substrate-binding proteins to scavenge nutrients is one such mechanism. Since SBPs form 50-80% of all proteins in the periplasm, a change in expression level could have major consequences for the crowding of the periplasm and the activity of SBP-dependent transporters. Apparently, the cell adjusts the volume of the periplasm to the amount of periplasmic proteins it synthesizes, thus keeping the concentration of SBPs relatively constant at all growth rates. The importance of controlling the level of expression of periplasmic SBPs is indicated by the observation that a modest change in the level of maltose-binding protein has an effect on the rate of maltose transport (Figure 8). The data are in accordance with a previous study on the dependence of maltose transport on the concentration of MBP [37]. There are approximately 20-40 MBPs present per transporter [17, 37]. From the copy number of MBP and the volume of the periplasm, the MBP concentration under non-inducing conditions is calculated to 20-40 μM . It has previously been shown that the affinity constant of MalFGK₂ for maltose-bound MBP is 25-50 μM [28]. Thus, under non-inducing conditions, the concentration of MBP is in the range of the affinity constant for its binding to the transporter, which makes the transport sensitive to changes in the concentration of MBP and warrants control of the periplasmic volume.

Our results show that a higher concentration of MPB indeed leads to faster uptake, the effect is however moderate. Theoretically the uptake could also be increased by upregulating the membrane transporter components MalFGK₂. We control the expression of *mal* genes by inducing with 10 μM maltose. We can however not exclude, that the differences between growth conditions emanate from variations in the levels of the transporter as a whole. From proteomics it seems that MalFGK₂ is constant under all growth conditions, however the variation in the data is large [17, 38]. The fact that we observe a higher rate of maltose transport in M9-acetate versus EZ-glycerol grown cells, even though the levels of MalE are similar, may reflect additional (allosteric) regulation of the transporter [39]. Gram-positive bacteria also have ABC transporters, however they only have one membrane and therefore lack the periplasmic space. Here, substrate-binding proteins are bound to the membrane surface via a lipid anchor or via a small flexible linker to the membrane components. Assuming that the function of SBPs is to increase the effective solute concentration near the transporter, Gram-positive bacteria would always have a high SBP concentration in the vicinity of the transporter.

In summary, we show that the fractional volume of the *E. coli* periplasm decreases and the cytoplasmic volume increases with increasing growth rate.

Proteins levels and cytoplasmic and periplasmic volumes are regulated in such a way that crowding conditions are kept constant at slow and fast growth. The impact of periplasmic protein concentration is shown for the transport of maltose via an ABC transporter.

References

1. Young KD (2006) The selective value of bacterial shape. *Microbiol Mol Biol Rev* **70**: 660-703
2. Tropini C, Lee TK, Hsin J, Desmarais SM, Ursell T, Monds RD, Huang KC (2014) Principles of bacterial cell-size determination revealed by cell-wall synthesis perturbations. *Cell Rep* **9**: 1520-1527
3. Pierucci O (1978) Dimensions of *Escherichia coli* at various growth rates: model for envelope growth. *J Bacteriol* **135**: 559-574
4. Grossman N, Ron EZ, Woldringh CL (1982) Changes in cell dimensions during amino acid starvation of *Escherichia coli*. *J Bacteriol* **152**: 35-41
5. Kubitschek HE, Friske JA (1986) Determination of bacterial cell volume with the Coulter Counter. *J Bacteriol* **168**: 1466-1467
6. Schaechter M, Maaløe O, Kjeldgaard N (1958) Dependency on medium and temperature on cell size and chemical composition during balanced growth of *Salmonella typhimurium*. *J Gen Microbiol* **19**: 592-606
7. Stock JB, Rauch B, Roseman S (1977) Periplasmic space in *Salmonella typhimurium* and *Escherichia coli*. *J Biol Chem* **252**: 7850-7861
8. Koch AL (1998) The biophysics of the gram-negative periplasmic space. *Crit Rev Microbiol* **24**: 23-59
9. Pilizota T, Shaevitz JW (2012) Fast, multiphase volume adaptation to hyperosmotic shock by *Escherichia coli*. *PLoS One* **7**: e35205
10. Van den Bogaart G, Hermans N, Krasnikov V, Poolman B (2007) Protein mobility and diffusive barriers in *Escherichia coli*: consequences of osmotic stress. *Mol Microbiol* **64**: 858-871
11. Biemans-Oldehinkel E, Mahmood NA, Poolman B (2006) A sensor for intracellular ionic strength. *Proc Natl Acad Sci U S A* **103**: 10624-10629
12. Booth IR (1985) Regulation of cytoplasmic pH in bacteria. *Microbiol Rev* **49**: 359-378
13. Mykytczuk N, Trevors J, Leduc L, Ferroni G (2007) Fluorescence polarization in studies of bacterial cytoplasmic membrane fluidity under environmental stress. *Prog Biophys Mol Biol* **95**: 60-82
14. Ruiz N, Kahne D, Silhavy TJ (2006) Advances in understanding bacterial outer-membrane biogenesis. *Nat Rev Microbiol* **4**: 57-66
15. Schulman H, Kennedy EP (1979) Localization of membrane-derived oligosaccharides in the outer envelope of *Escherichia coli* and their occurrence in other Gram-negative bacteria. *J Bacteriol* **137**: 686-688
16. Kennedy EP (1982) Osmotic regulation and the biosynthesis of membrane-derived oligosaccharides in *Escherichia coli*. *Proc Natl Acad Sci U S A* **79**: 1092-1095
17. Schmidt A, Kochanowski K, Vedelaar S, Ahrné E, Volkmer B, Callipo L, Knoops K, Bauer M, Aebersold R, Heinemann M (2015) The quantitative and condition-dependent *Escherichia coli* proteome. *Nat Biotechnol* **34**: 104-110
18. Lim KH, Huang H, Pralle A, Park S (2011) Engineered streptavidin monomer and dimer with improved stability and function. *Biochemistry* **50**: 8682-8691

19. Datsenko KA, Wanner BL (2000) One-step inactivation of chromosomal genes in *Escherichia coli* K-12 using PCR products. *Proc Natl Acad Sci U S A* **97**: 6640-6645
20. DeMonte D, Drake EJ, Lim KH, Gulick AM, Park S (2013) Structure-based engineering of streptavidin monomer with a reduced biotin dissociation rate. *Proteins* **81**: 1621-1633
21. Mika JT, Krasnikov V, Van den Bogaart G, de Haan F, Poolman B (2011) Evaluation of pulsed-FRAP and conventional-FRAP for determination of protein mobility in prokaryotic cells. *PLoS One* **6**: e25664
22. Thomas JD, Daniel RA, Errington J, Robinson C (2001) Export of active green fluorescent protein to the periplasm by the twin-arginine translocase (Tat) pathway in *Escherichia coli*. *Mol Microbiol* **39**: 47-53
23. Berks BC (2015) The twin-arginine protein translocation pathway. *Annu Rev Biochem* **84**: 843-864
24. Barrett CM, Ray N, Thomas JD, Robinson C, Bolhuis A (2003) Quantitative export of a reporter protein, GFP, by the twin-arginine translocation pathway in *Escherichia coli*. *Biochem Biophys Res Commun* **304**: 279-284
25. Sochacki KA, Shkel IA, Record MT, Weisshaar JC (2011) Protein diffusion in the periplasm of *E. coli* under osmotic stress. *Biophys J* **100**: 22-31
26. Boersma AJ, Zuhorn IS, Poolman B (2015) A sensor for quantification of macromolecular crowding in living cells. *Nat Methods* **12**: 227-229
27. Szmelcman S, Schwartz M, Silhavy TJ, Boos W (1976) Maltose transport in *Escherichia coli* K12. *Euro J Biochem* **65**: 13-19
28. Dean DA, Hor LI, Shuman HA, Nikaido H (1992) Interaction between maltose-binding protein and the membrane-associated maltose transporter complex in *Escherichia coli*. *Mol Microbiol* **6**: 2033-2040
29. Graham L, Beveridge T, Nanninga N (1991) Periplasmic space and the concept of the periplasm. *Trends Biochem Sci* **16**: 328-329
30. Matias VR, Al-Amoudi A, Dubochet J, Beveridge TJ (2003) Cryo-transmission electron microscopy of frozen-hydrated sections of *Escherichia coli* and *Pseudomonas aeruginosa*. *J Bacteriol* **185**: 6112-6118
31. Kubori T, Matsushima Y, Nakamura D, Uralil J, Lara-Tejero M, Sukhan A, Galan JE, Aizawa SI (1998) Supramolecular structure of the *Salmonella typhimurium* type III protein secretion system. *Science* **280**: 602-605
32. Murakami S, Nakashima R, Yamashita E, Yamaguchi A (2002) Crystal structure of bacterial multidrug efflux transporter AcrB. *Nature* **419**: 587-593
33. Koronakis V, Sharff A, Koronakis E, Luisi B, Hughes C (2000) Crystal structure of the bacterial membrane protein TolC central to multidrug efflux and protein export. *Nature* **405**: 914-919
34. Mika JT, Van Den Bogaart G, Veenhoff L, Krasnikov V, Poolman B (2010) Molecular sieving properties of the cytoplasm of *Escherichia coli* and consequences of osmotic stress. *Mol Microbiol* **77**: 200-207
35. Konopka MC, Shkel IA, Cayley S, Record MT, Weisshaar JC (2006) Crowding and confinement effects on protein diffusion in vivo. *J Bacteriol* **188**: 6115-6123
36. Dix JA, Verkman A (2008) Crowding effects on diffusion in solutions and cells. *Annu Rev Biophys* **37**: 247-263
37. Manson MD, Boos W, Bassford PJ, Jr, Rasmussen BA (1985) Dependence of maltose transport and chemotaxis on the amount of maltose-binding protein. *J Biol Chem* **260**: 9727-9733
38. Li G, Burkhardt D, Gross C, Weissman JS (2014) Quantifying absolute protein synthesis rates reveals principles underlying allocation of cellular resources. *Cell* **157**: 624-635
39. Chen S, Oldham ML, Davidson AL, Chen J (2013) Carbon catabolite repression of the maltose transporter revealed by X-ray crystallography. *Nature* **499**: 364-368

